AIP Advances

Magnetic and nonlinear optical properties of BaTiO3 nanoparticles

S. Ramakanth, Syed Hamad, S. Venugopal Rao, and K. C. James Raju

Citation: AIP Advances **5**, 057139 (2015); doi: 10.1063/1.4921480
View online: http://dx.doi.org/10.1063/1.4921480
View Table of Contents: http://scitation.aip.org/content/aip/journal/adva/5/5?ver=pdfcov
Published by the AIP Publishing

AIP ADVANCES **5**, 057139 (2015)

Magnetic and nonlinear optical properties of $BaTiO_3$ nanoparticles

S. Ramakanth,[1] Syed Hamad,[2] S. Venugopal Rao,[1,a] and K. C. James Raju[1,2,b]
[1]*Advanced Centre of Research in High Energy Materials* ***(ACRHEM),*** *University of Hyderabad, Hyderabad 500046, Telangana, India*
[2]*School of Physics, University of Hyderabad, Hyderabad 500046, Telangana, India*

(Received 16 March 2015; accepted 11 May 2015; published online 20 May 2015)

In our earlier studies the $BaTiO_3$ samples were processed at higher temperatures like 1000ºC and explained the observed magnetism in it. It is found that the charge transfer effects are playing crucial role in explaining the observed ferromagnetism in it. In the present work the samples were processed at lower temperatures like 650ºC-800ºC. The carrier densities in these particles were estimated to be ~ 10^{19}-10^{20}/cm^3 range. The band gap is in the range of 2.53eV to 3.2eV. It is observed that magnetization increased with band gap narrowing. The higher band gap narrowed particles exhibited increased magnetization with a higher carrier density of 1.23×10^{20}/cm^3 near to the Mott critical density. This hint the exchange interactions between the carriers play a dominant role in deciding the magnetic properties of these particles. The increase in charge carrier density in this undoped $BaTiO_3$ is because of oxygen defects only. The oxygen vacancy will introduce electrons in the system and hence more charge carriers means more oxygen defects in the system and increases the exchange interactions between Ti3+, Ti4+, hence high magnetic moment. The coercivity is increased from 23 nm to 31 nm and then decreased again for higher particle size of 54 nm. These particles do not show photoluminescence property and hence it hints the absence of uniformly distributed distorted [TiO5]-[TiO6] clusters formation and charge transfer between them. Whereas these charge transfer effects are vital in explaining the observed magnetism in high temperature processed samples. Thus the variation of magnetic properties like magnetization, coercivity with band gap narrowing, particle size and charge carrier density reveals the super paramagnetic nature of $BaTiO_3$ nanoparticles. The nonlinear optical coefficients extracted from Z-scan studies suggest that these are potential candidates for optical imaging and signal processing applications. [http://dx.doi.org/10.1063/1.4921480]

I. INTRODUCTION

Spintronic device implementations require the study of functional properties of semiconducting oxides, as the coupled electronic, magnetic and optical properties in these materials are to be utilised. In dilute magnetic semiconductor oxides the cations are partially replaced by transition metal ions. These materials show strong exchange interactions between charge carriers of semiconductor and doped transition metal d electrons. These types of interactions are vital in determining the spin dependent electrical and optical properties.[1] Size reduction of these materials is essential in understanding the origin and type of interactions in these materials. The optical properties are important in studying the magnetic semiconductors because the doping dependent optical properties like optical

[a]e-mail: svrsp@uohyd.ernet.in
[b]e-mail: kcjrsp@uohyd.ernet.in

absorption (optical band gap) and Z-scan studies reveal the presence of carriers in the valence and conduction bands. The different amount of doping in semiconductors produces respective amount of free carriers in the material. Depending on their concentration, these carriers create signatures in their optical absorption spectrum by demonstrating various effects like band gap narrowing, band gap widening or bleaching of optical absorption. In addition, the Z-scan measurements also reflect the carrier concentration dependent changes in their nonlinear refractive index (n_2).

As discussed above similar to doped semiconductors, the various concentrations of charge carriers are created through oxygen defects in oxide nanoparticles. The study of charge carriers in these wide band gap oxide nanoparticles is quite difficult through standard measurements like Hall Effect alone. Hence the optical measurements like UV/VIS/NIR absorption and Z-scan techniques are effective methods in studying the charge carrier effects in them. The Z-scan technique is used to calculate the free carrier concentration in these nanoparticles.

It is known that the electron-phonon interactions also play an active role when the size of the materials goes to nanometer scale. The electron-phonon interactions and electron-electron interactions are well studied in nanomaterials to explain their optical properties too. But the particular interaction responsible for occurrence of ferromagnetic phase in these nanomaterials is still under investigation. Recently observed ferromagnetism in ferroelectric[2–6] nanomaterials,[7–13] makes the ferromagnetism as a trivial property of nanomaterials.[14] The most common property of these materials is that they don't have unpaired electrons in them, but still show magnetism which is counter intuitive. Magnetism in ferroelectric materials brings forth an idea of doping ferroelectric materials with magnetic and nonmagnetic ions to study their ferroelectric and ferromagnetic properties.[15,16] It is expected that such studies will help in coupling the ferromagnetic and ferroelectric property based applications in a single device like electric field tuning of magnetic properties which is required for devices but difficult.

The understanding of magnetism in dilute magnetic semiconductor (DMS) is based on free carriers and is a very broadly accepted concept. According to this, the ferromagnetism in TM–ZnO (TM = Sc, Ti, V, Cr, Mn, Co, Ni, and Cu) is due to the exchange interactions between the sp band charge carriers and localised d-electrons.[17,18] When the electron concentration crosses the critical value for the above system, the ferromagnetic interactions reduces.[19] Hence the p-d hybridization is crucial in describing the observed magnetism in the above systems.[20–25] The common feature for dilute magnetic semiconductors and defect based magnetism in oxide materials is the density of charge carriers.

Barium titanate (BTO), and lanthanum strontium magnese oxide (LSMO), ferroelectric and ferromagnetic bilayer based multiferroics are presently constantly explored materials. But these films are not compatable with Silicon because of the diffusivity of film material into the silicon. Presently the research heavily focussed to bypass this problem by various routes. One of them is the making BTO itself ferromagnetic by creating defects in it.[26] And hence the study of origin of magnetism in BTO is highly involved. In our earlier work we have explicitly explained how different methods in various compounds lack the full explanation for the magnetism in d^0 materials. We have also pointed out that the theoretically obtained values for magnetic moment is not matching with experimental results. To consider these facts more decently we have taken the charge transfer concept in these perovskite materials (which arises from the oxygen defects) and explained the magnetism in nanocrystalline BTO.[27] Here we also considered how the exchange interactions are arising in nanocrystalline BTO and its role in setting up the magnetic ground state for the system.[27] Here in the present paper we considered the case where charge transfer is absent, as these samples do not show photoluminescence. As we know the disordered BTO or defective BTO nanoparticles photoluminescence is explained very well by considering the formation of [TiO6] and [TiO5] clusters in the material.[28] In this case the charge transfer takes place from [TiO5] cluster to [TiO6] cluster and hence changes the Ti valence state from Ti^{+4} to Ti^{+3} or even more. Here the BTO do not show the photoluminescence peak and hence uniformly distributed distorted [TiO5]-[TiO6] cluster formation is absent in these samples and confirms the absence of charge transfer effects in it, and hence the anti ferromagnetic contribution is dominant. Thus, as mentioned above, the charge carriers play a crucial role in determining the electronic, optical and magnetic properties in semiconductors. Here we have carried out the magnetic studies like M-H loop, zero field cooled

and field cooled (ZFC-FC) measurements for four different sizes of $BaTiO_3$ (BTO) nanoparticles. The Z-scan measurements were carried out to calculate the free carrier density and its effects on nonlinear optical (NLO) coefficients. The UV/VIS/NIR optical absorption and Z-scan studies shows very good agreement with magnetic studies and helps in understanding the observed magnetism in BTO nanoparticles. NLO coefficients extracted from closed/open aperture data indicate potential of these materials in various applications.

II. EXPERIMENTAL

BTO nanoparticles of various sizes were prepared using sol-gel method,[29–31] by taking barium acetate and titanium isopropoxide as precursor chemicals. The BTO nanoparticles of different sizes were obtained by calcining the dried sol at 650ºC-800ºC temperature range for 1hr. The details of preparation of these particles were briefly discussed in our earlier paper.[27] The structural and micro structural characterization is carried out by Transmission electron microscopy (Tecnai 20 G2 STwin, FEI electron microscope) operated at 200 KV. The magnetic measurements were carried out using a 6000 PPMS (Vibrating Sample Magnetometer, Quantum Design Instruments). The carrier concentration studies were carried out by Z-scan technique under the conditions given below. The Z-scan experiments were performed with ps pulses which were generated by separate Ti: sapphire laser (Coherent, Legend amplifiers) operating at a repetition rate of 1 kHz with pulse duration of ~2 ps at 800 nm. The amplifiers were seeded with ~15 fs pulses from an oscillator (Coherent, Micra). The input beam was spatially filtered using a pin hole to obtain a pure Gaussian profile in the far field. Z-scan studies[32–36] were performed by focusing a 3-mm diameter input beam using a 200 mm focal length convex lens into the sample in both ps domain. The sample was placed on a high resolution linear translation stage and the detector (Si photodiode, SM1PD2A, Thorlabs) output was connected to a lock-in amplifier. Both the stage and lock-in were controlled by a computer program. The ps Z-scan studies were performed with these different size BTO particle dispersed PVA (polyvinyle alcohol) films with 80±10 μm thickness. All samples displayed 50-55 % linear transmittance at 800 nm wavelength. The experiments were repeated more than once and the best data were used for obtaining the NLO coefficients from the theoretical fits.

III. RESULTS AND DISCUSSIONS

A. DISCUSSION ON STRUCTURAL STUDIES

Structural characterization of these particles is carried out using Transmission electron microscopy. The samples show good XRD patterns without any amorphous contribution to it. The XRD patterns are given below in fig. 1(e). From the HRTEM images also clear that even at nanoparticle boundaries the particles is having clear lattice planes without any amorphous nature. In most of the chemical synthesis processes the crystallization temperature for $BaTiO_3$ is in the range of 600ºC-700ºC.[28,37–40] Basically the higher temperatures are used for grain growth and densification in the sintering process.

Inset in Figure 1(a)-1(d) clearly shows the nano range size of BTO particles at avg. sizes of ~23 nm, ~31 nm, ~34 nm and ~54 nm. Figure 1(a)-1(d) shows the HRTEM images of all four particle size ranges. All the patterns show the presence of $BaTiO_3$ crystal planes. The corresponding d values are given in respective figures [Figures 1(a)-1(d)]. The particles having some size distribution and arbitrary shape, the avg. size is got for the distribution particles shown in inset of Fig. 1. We have taken some HRTEM images for corresponding to higher size particles also. The small particle HRTEM images not only address the phase formation but also it evidences the higher crystallinity by showing sharp lattice planes at small particle boundaries also. The energy dispersive X-ray analysis (EDS) measurements also rules out the presence of magnetic impurities in these samples.

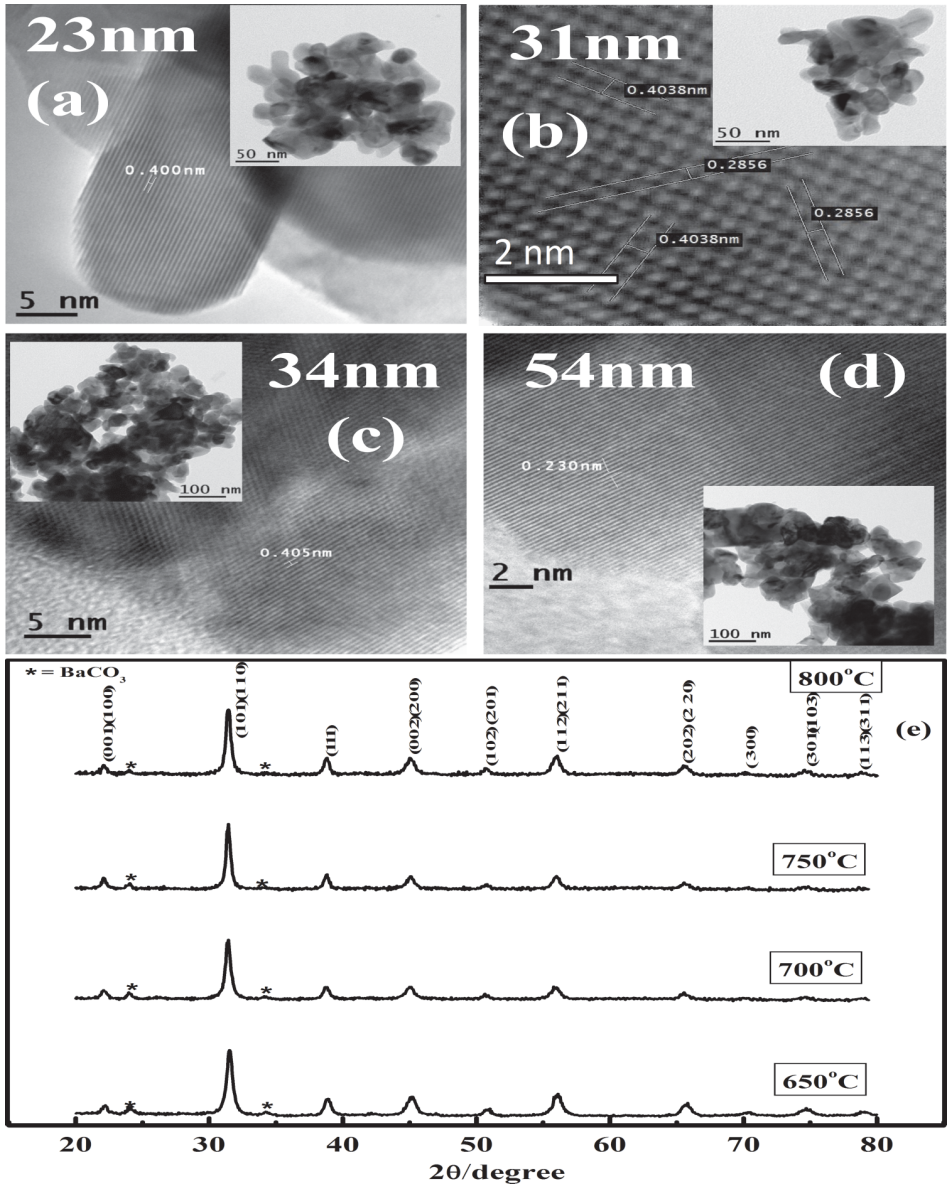

FIG. 1. HRTEM images of BTO nanoparticles. The Insets Figures 1(a)–1(d), show the TEM images of BTO nanoparticles of avg. sizes (a) ~23 nm, (b) ~31 nm, (c) ~34 nm and (d) ~54 nm. (e) XRD patterns of different temperature synthesized above four different size particles.

B. NLO PROPERTIES/STUDIES

Open Aperture Z-scan

The open aperture data obtained were fitted initially for pure two photon absorption (2PA). We combine the linear and two 2PA (β) coefficients giving a total absorption coefficient[41] as

$$\alpha(I) = \alpha_0 + \beta I \tag{1}$$

Where α_0 is the linear absorption coefficient. $I = I(z) = I_{00}/(1 + \frac{z^2}{z_0{}^2})$ is the excitation intensity at position z and I_{00} is the peak intensity.

2PA coefficient (β) can be obtained by fitting the following equation

$$\frac{dI}{dz} = -\alpha(I)l \tag{2}$$

Substitute eq (1) in eq (2), then

$$\frac{dI}{dz} = -\alpha_0 I - \beta I^2 \tag{3}$$

The transmitted intensity equation through the sample after solving the above differential equation is named as $I_f(z)$ and the normalized transmittance can be formulated as $T(z) = I_f(z)/I(z)$

The final equation of the transmitted intensity for 2PA is

$$T(z) = 1 - \frac{\beta I_{00} L_{eff}}{2^{3/2}(1 + (z/z_0)^2)} \tag{4}$$

Where $L_{eff} = \frac{1-e^{-\alpha_0 L}}{\alpha_0}$ and L = sample length

(ii) To interpret the switching of saturable absorption (SA) in reverse saturable absorption (RSA) in the open aperture data we combine both the coefficients of SA and 2PA (β) which yield to the total absorption coefficient[41,42] given by

$$\alpha(I) = \frac{\alpha_0}{1 + I/I_s} + \beta I \tag{5}$$

I_s and β can be obtained by fitting the following equation (2)

$$\frac{dI}{dz} = -\frac{\alpha_0}{1 + \frac{I}{I_s}} I - \beta I^2 \tag{6}$$

Where I_s is the saturation intensity.

The transmitted intensity equation through the sample after solving the differential equation (using matlab-ODE45) is named as $I_f(z)$ and the normalized transmittance can be formulated as $T(z) = I_f(z)/I(z)$

Closed Aperture Z-scan

Similarly the normalized closed aperture transmittance can be determined as follows

$$T(\frac{z}{z_0}) = 1 - \frac{4\left(\frac{z}{z_0}\right)\Delta\phi_0}{\left[\left(\frac{z}{z_0}\right)^2 + 1\right]\left[\left(\frac{z}{z_0}\right)^2 + 9\right]} \tag{7}$$

Where Z is the sample position, $z_0 = \pi\omega_0{}^2/\lambda$ is the Rayleigh range: ω_0 is the beam waist at the focal point (Z=0), λ is the wavelength; $\Delta\phi_0$ is the nonlinear phase shift

Figures 2(a) – 2(d) show the open aperture Z-scan data of particles with average sizes of ~23 nm, ~31 nm, ~34 nm and ~54 nm, respectively, (calcined in the range of 650 ºC - 800 ºC) recorded at a peak intensity of 140 GW/cm^2. The data in figures 2(a) and 2(c) indicate simple reverse saturable absorption while the data in figures 2(b) and 2(d) demonstrated complex behaviour with switching from saturable absorption (SA) to reverse saturable absorption (RSA). A good fit was obtained for dominant two-photon absorption coefficient (β) with magnitude of the order of 10^{-9} cm/W and saturation intensity (I_s of ~ of 10^8 W/cm^2) was also calculated for particles sized ~31 nm and ~54 nm. No specified nonlinear absorption was observed from the PVA substrate. Solid (blue) lines in the figure 2 are theoretical fits.

Closed aperture data along with the corresponding theoretical fits (red, solid lines) for average size of (a) ~23 nm, (b) ~31 nm, (c) ~34 nm and (d) ~54 nm particles is shown in figures 3(a)-3(d), respectively. The closed aperture scans for all the samples were recorded with a peak intensity of 80 GW/cm^2. Open circles represent the experimental data for nanoparticles while the solid lines are the theoretical fits.[32–36,43] In the case of particles of size ~31 nm, the sign of nonlinear refraction n_2 was negative. But in all the other cases, the sign of nonlinearity was positive. We obtained the best fit for n_2 with a magnitude of ~10^{-13} cm^2/W. All the nonlinear coefficients are summarized in table I.

By using the above fitted parameters we calculated the charge carrier density (N_e) for all these particles using the following relation.[44,45]

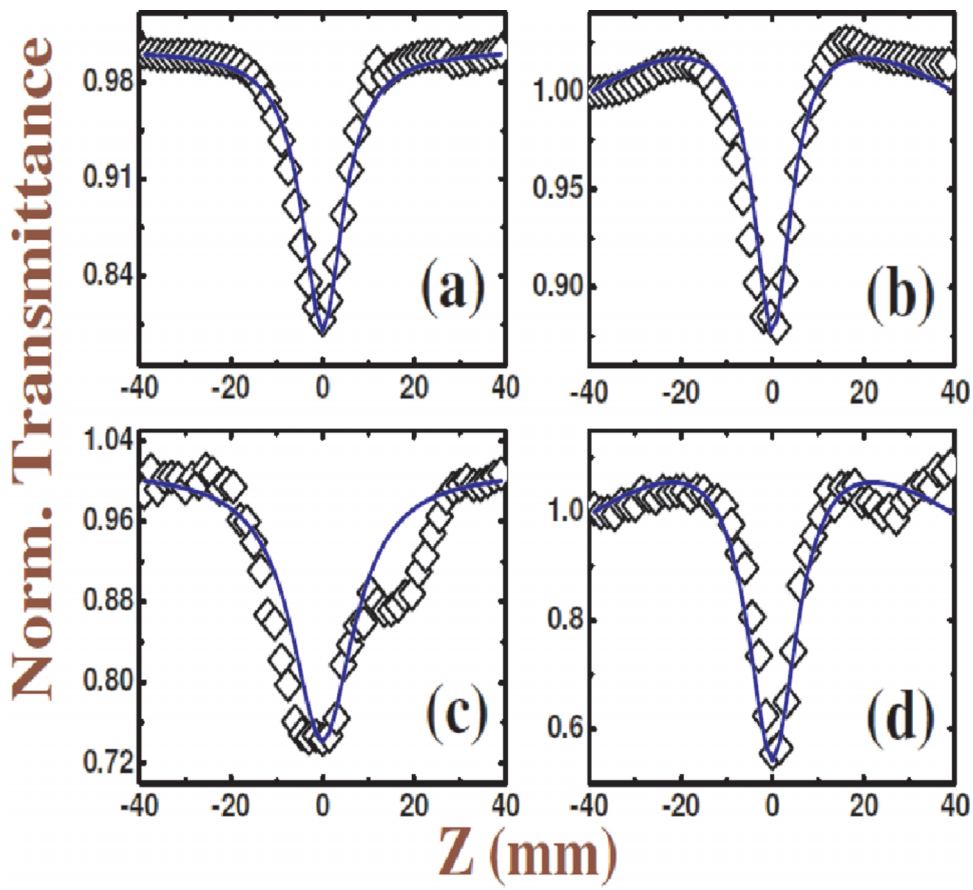

FIG. 2. Open aperture Z-scan curves obtained for Particles of avg. sizes of (a) ~23 nm and (b) ~31 nm (c) ~34 nm and (d) ~54 nm at a peak intensity of $I_{00} = 140$ GW/cm^2. Open squares are experimental points and Blue solid line represent the theoretical fit.

$$N_e = F\frac{(1-T)}{h\nu}\left[\alpha + \beta F\frac{(1-T)}{((2\sqrt{\pi})\tau)}\right]$$

where F = Fluence, T = Linear transmittance, τ= pulse width and α=linear absorption.

It was observed that higher band gap narrowed samples show higher charge carrier density as expected. Thus we obtained the concentrations as ~ 8.09×10^{19}/cm^3, ~8.17×10^{19}/cm^3 and ~9.06×10^{19}/cm^3 concentration for particles of sizes ~23 nm, ~31 nm, and ~34 nm respectively. The higher charge density of ~ 1.29×0^{20}/cm^3 was obtained for ~54 nm particles (Table I). This is nearer to the Mott critical density for BTO.[46–48]

In the refractive index sign change of these kinds of materials, the main factors involved are electronic Kerr effect, optical electrostriction, population redistribution and thermal contribution. Generally thermal heat induced refractive index change will be negative, but the response time will be high in the nanosecond (ns) range. As we know that the time scale for the energy exchange between the electrons is few fs-100ps and for electron-phonons typically are ~ns. In the present studies we have used ps pulses and since the effects relax at ps time scales the observed refractive index change is expected to be electronic in origin. Except in the case of ~34 nm size particles (with E_g = 3.2 eV), all other particles displayed small band gap values compared to the band gap of bulk BTO (3.2 eV). But the bleaching of absorption spectrum in particles of this size is evident for the presence of certain concentration of free carriers induced conduction band filling in them.[49]

As summarized in table I, the band gap of these particles varied in the range of 2.53eV - 3.2eV. The samples with higher band gap narrowing demonstrated enhanced optical absorption. The higher band gap narrowing is due to the exchange-correlation interactions between the carriers. The band

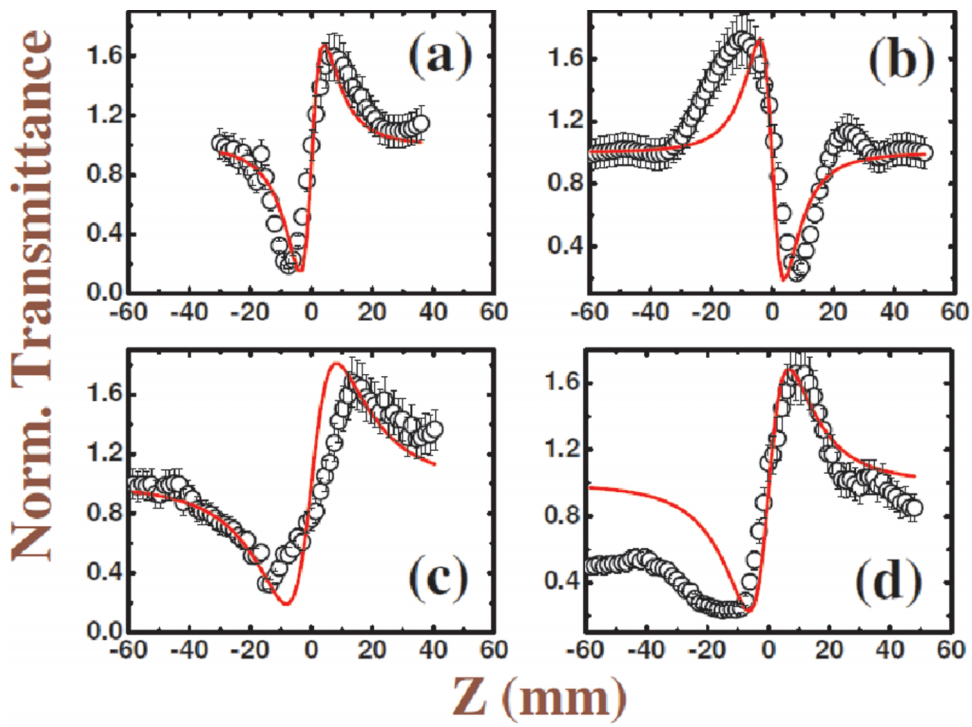

FIG. 3. Closed aperture Z-scan curves recorded for Particles of avg. sizes of (a) ~23 nm (b) ~31 nm (c) ~34 nm and (d) ~54 nm at a peak intensity of $I_{00} = 140$ GW/cm^2. Open stars are experimental points and orange solid line represent the theoretical fit.

gap narrowing and involved mechanisms were discussed in our earlier paper.[49] Since the higher value for N_e is obtained from Z-scan measurements for all particles, in addition to some of the particles displaying narrowed band, with negative refractive index (n_2) and bleached optical absorption, the presence of higher concentrations of charge carriers in these particles can be concluded.[50–53] The higher band gap for these particles is expected due to the mixing up of O 2p states in the valence band and Ti 3d states in the conduction band. This mixing increases the effective mass of electrons in the conduction band and hence there is now effective band narrowing like the other two particle sizes. The magnetic measurements also support these results and will be discussed in the next section.

TABLE I. Observed nonlinear coefficients of particles of average sizes of ~23 nm, ~31 nm, ~34 nm and ~54 nm.

Calcination Temp. (°C)	Avg. particle size (D) nm	Band gap (eV)	β 10^{-9} (cm/W)	n_2 10^{-13} (cm^2/W)	Charge carrier density (N_e)/cm^3	$M_s \times 10^{-3}$ emu/gm) (M_s= saturation magnetization)	H_c (Oe) H_c=coercivity
650	23	2.83	0.85 (140 GW/cm^2)	1	8.09×10^{19}	2.2	58
700	31	3.00	0.17 (140 W/cm^2) $I_S = 1\times10^8$ W/cm^2	-0.9	8.17×10^{19}	1.4	60
750	34	3.2	1.5 (140 GW/cm^2)	0.9	9.06×10^{19}	1.3	68
800	54	2.53	1.2 (140 W/cm^2) $I_S = 4\times10^8$ W/cm^2	1	1.29×10^{20}	3.2	54

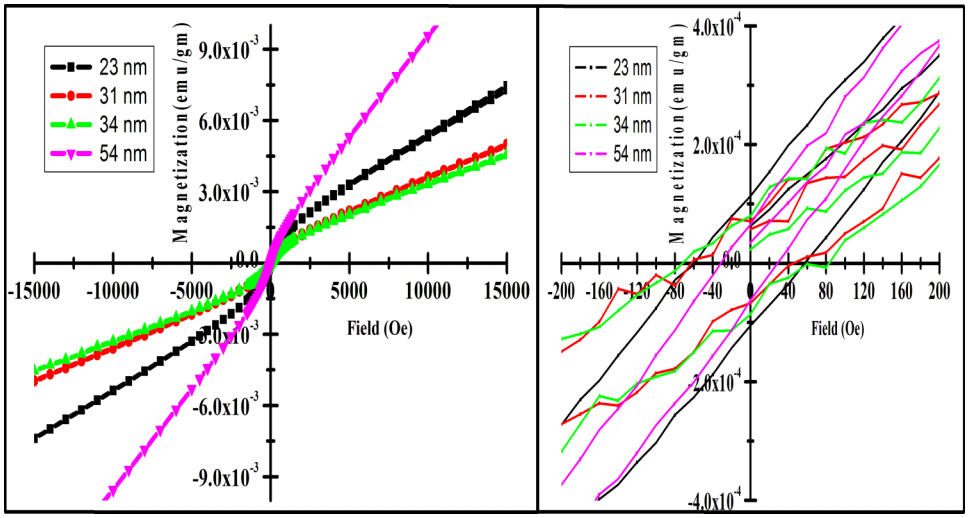

FIG. 4. (Left) M-H curves for particles of different sizes (23 nm- 54 nm) at 300K. (Right) shows the coercivity values.

C. MAGNETIC PROPERTIES

The field dependent magnetization (M-H) measurements were carried out for all these four different sizes of particles at 300 K (figure 4.). The coercivity increases from 55 Oe to 70 Oe as the particle size increases from ~23 nm to ~34 nm. Further increament in particle size to 54 nm leads to a drastic reduction in coercivity to 28 Oe (figure 5. right). From figure 4 the drastic coercivity and remanence decrease for 54 nm size particle suggests the presence of strong interparticle interactions compared to the other three particle sizes.[54] For ZFC measurements the material is cooled to 2K at H=0 Oe, and then the magnetic moment is measured with increasing temperature. In the FC case the sample is cooled to 2K in presence of 1KOe applied field and then magnetic moment is measured while warming. Figure 5. shows FC-ZFC curves for particles of all four sizes. The particles of sizes ~23 nm, ~34 nm and ~54 nm showed higher bifurcation temperature, whereas the ~31 nm size particles show lower bifurcation temperature. A clear additional peak around 19K is observed for 34 nm size particles, which may be due to the critical temperature for the surface spins alignment along the core spin of the particle.[55]

The optical measurements like, optical absorption and Z-scan measurements shows the band gap filling by carriers in ~31 nm and ~34 nm size particles. Whereas the particles of ~23 nm and ~54 nm sizes show enhanced absorption with narrowed band gap. It was noted that the ~31 nm size particles exhibited lower magnetic moment and lower bifurcation temperature. The concave like trend of ZFC is also diminished in 31nm size particle. The magnetization was increased with reduction in band gap (right side in Figure 5). i. e. lower band gap particles showed higher saturation

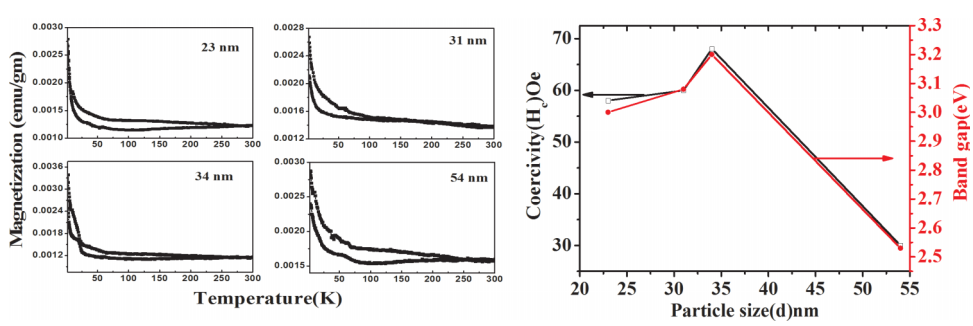

FIG. 5. ZFC-FC (M vs T) curves for different sizes of nanoparticles. Figure 5 (right side) gives variation of coercivity and band gap with particle size of BTO nanoparticles.

magnetization and higher band gap particles showed lower saturation magnetization.[56] As discussed above the higher charge carrier concentration leads electrons to get localised to Ti site and reduces its oxidation state further.

The Z-scan and optical absorption techniques turn out to be two very simple and important techniques in constructive understanding of magnetism in these particles. As discussed above, the particles of size ~31 nm showed negative n_2 of 0.9×10^{-13} cm^2/W, whereas all other particles depicted positive n_2. This negative refractive index also clearly indicates the higher concentration of free carriers in these particles.

The bifurcation temperature (T_b) in these particles also reduced to 150K. Whereas the particles of sizes ~23 nm, ~34 nm and ~54 nm displayed higher bifurcation temperatures in the range of 250K-270K. Thus, different bifurcation temperatures were observed for four different sizes of particles. It is clear that depending upon the charge carrier density, different interactions occur in these nanomaterials. This indirectly is reflected in the varying electron concentration of charge carriers and the presence of different band gaps.[57]As discussed above the ~54 nm size particles displayed higher charge carrier density. The mixing up of O 2P and Ti 3d states causes the higher band gap widening in ~31 nm and ~34 nm size particles.[58,59] Therefore, we expect that higher concentration of charge carriers provide larger magnetic moment and it is supported by the band gap narrowing due to exchange-correlation interactions between the carriers.[56]

IV. CONCLUSIONS

It is concluded that the charge carrier density is crucial in understanding the observed magnetism in BTO nanoparticles. The magnetic moment has increased as the band gap of the particles decreased. The particles with average sizes of ~31 nm and ~34 nm did not show marginal band gap narrowing. Thus it can be said that the O 2p and Ti 3d states were mixed to yield a counter renormalization of band gap due to increase of the electron effective mass. Therefore, the increased charge carrier concentration increased the magnetic moment values due to the dominant exchange interactions between the carriers. And, hence, band gap narrowing was observed for higher carrier density. These arguments are also supported by the Z-scan measurements where one of the samples showed negative refractive index (n_2) in addition to the higher charge carrier density in them. It also confirms the large charge carrier density present in them. The ZFC-FC measurements show the lower bifurcation temperature (T_b) of 150K for 31nm size particles. The ~23 nm, ~34 nm and ~54 nm size particles showed higher bifurcation temperatures in the range of 250K-270K. Thus the higher carrier density samples displayed higher magnetic moment with lower band gap values due to the exchange correlation interactions between the carriers.

ACKNOWLEDGEMENTS

We would like to acknowledge DST, New Delhi for a fellowship, as well as UGC and DST for providing TEM, VSM facilities at Centre for Nano Technology (CFN) at UOH. SVR thanks DRDO for continued financial support.

[1] J K Furdyna, "Diluted magnetic semiconductors," J. Appl. Phys. **64**, R29 (1988).

[2] R V K Mangalam, N Ray, U V Waghmare, A Sundaresan, and C N R Rao, "Multiferroic properties of nanocrystalline $BaTiO_3$," Solid State Commun. **149**, 1-5 (2009).

[3] D Cao, M Q Cai, W Y Hu, P Yu, and H T Huang, "Vacancy-induced magnetism in BaTiO3(001) thin films based on density functional theory," Phys. Chem. Chem. Phys. **13**, 4738-4745 (2011).

[4] T Shimada, Y Uratani, and T Kitamura, "Vacancy-driven ferromagnetism in ferroelectric PbTiO3'," Appl. Phys. Lett. **100**, 162901 (2012).

[5] K Potzger, J Osten, A A Levin, A Shalimov, G Talut, H Reuther, S Arpaci, D Burger, H Schmidt, T Nestler, and D C Meyer, "Defect-induced ferromagnetism in crystalline SrTiO3," J. Magn. Magn. Mater. **323**(11), 1551-1561 (2011).

[6] Shilpi Banerjee, Anindya Datta, Asim Bhaumik, and Dipankar Chakravorty, "Multiferroic behaviour of nanoporous BaTiO3," J. Appl. Phys. **110**, 064316 (2011).

[7] J M D Coey, P Stamenov, R D Gunning, M Venkatesan, and K Paul, "Ferromagnetism in defect-ridden oxides and related materials," New. J. Phys. **12**, 053025 (2010).

[8] Peng Zhan, Zheng Xie, Zhengcao Li, Weipeng Wang, Zhengjun Zhang, Zhuoxin Li, Guodong Cheng, Peng Zhang, Baoyi Wang, and Xingzhong Cao, "Origin of the defects-induced ferromagnetism in un-doped ZnO single crystals," Appl. Phys. Lett. **102**, 071914 (2013).
[9] P Crespo, R Litra'n, T C Rojas, M Multigner, J M de la Fuente, J C Sa'nchez-Lo'pez, M A Garcı'a, A Hernando, S Penade's, and A Ferna'ndez, "Permanent Magnetism, Magnetic Anisotropy, and Hysteresis of Thiol-Capped Gold Nanoparticles," Phys. Rev. Lett. **93**, 087204 (2004).
[10] Shengqiang Zhou, E. Čižmár, K. Potzger, M. Krause, G. Talut, M. Helm, J. Fassbender, S. A. Zvyagin, J. Wosnitza, and H. Schmidt, "Origin of magnetic moments in defective TiO2 single crystals," Phys. Rev. B **79**, 113201 (2009).
[11] Nguyen Hoa Hong, Joe Sakai, Nathalie Poirot, and Virginie Brizé, "Room-temperature ferromagnetism observed in undoped semiconducting and insulating oxide thin films," Phys. Rev. B **73**, 132404 (2006).
[12] Soack Dae Yoon, Yajie Chen, Aria Yang, Trevor L Goodrich, Xu Zuo, Dario A Arena, Katherine Ziemer, Carmine Vittoria, and Vincent G Harris, "Oxygen-defect-induced magnetism to 880 K in semiconducting anatase TiO2−δ films," J. Phys.: Condens. Matter **18**, L355 (2006).
[13] J M D Coey, "d0 ferromagnetism," Solid State Sci. **7**(6), 660-667 (2005).
[14] A Sundaresan, R Bhargavi, N Rangarajan, U Siddesh, and C N R Rao, "Ferromagnetism as a universal feature of nanoparticles of the otherwise nonmagnetic oxides," Phys. Rev. B **74**, 161306R (2006).
[15] N V Dang, T-L Phan, T D Thanh, V D Lam, and L V Hong, "Structural phase separation and optical and magnetic properties of BaTi1–xMnxO3 multiferroics," Appl. Phys. Lett. **111**, 113913 (2012).
[16] C Gruber, P O B Velazquez, J Redinger, P Mohn, and M Marsman, "p-electron magnetism in doped BaTiO3-xMx (M=C, N, B)," E. Phys. Lett. **97**, 67008 (2012).
[17] K Ando, H Saito, Z Jin, T Fukumura, M Kawasaki, Y Matsumoto, and H Koinuma, "Large magneto-optical effect in an oxide diluted magnetic semiconductorZn1-xCoxO," Appl. Phys. Lett. **78**, 7200 (2001).
[18] A L Ivanovskii, Phy. Uspekhi **50**, 1031 (2007).
[19] Ashutosh Tiwari, Michael Snure, Dhananjay Kumar, and Jeremiah T. Abiade, "Ferromagnetism in Cu-doped ZnO films: Role of charge carriers," Appl. Phys. Lett. **92**, 062509 (2008).
[20] D Chakraborti, J Narayan, and J T Prater, "Room temperature ferromagnetism in Zn1–xCuxO thin films," Appl. Phys. Lett. **90**, 062504 (2007).
[21] S E Thomas Wolfram, *Electronic and optical properties of d-band perovskites* (Cambridge University Press, New York, 2006).
[22] Hyeon-Jun Lee, Bo-Seong Kim, Chae Ryong Cho, and Se-Young Jeong, "A study of magnetic and optical properties of Cu-doped ZnO," Phys. Stat. Sol. (b) **241**, 1533 (2004).
[23] Y S Wang, P J Thomas, and P O Brien, "Optical Properties of ZnO Nanocrystals Doped with Cd, Mg, Mn, and Fe Ions," J. Phys. Chem. B **110**, 21412 (2006).
[24] Ranjani Viswanatha, Sameer Sapra, Subhra Sen Gupta, B. Satpati, P. V. Satyam, B. N. Dev, and D. D. Sarma, "Synthesis and Characterization of Mn-Doped ZnO Nanocrystals," J. Phys. Chem. B **108**, 6303 (2004).
[25] M Ferhat, A Zaoui, and R Ahuja, "Magnetism and band gap narrowing in Cu-doped ZnO," Appl. Phys. Lett. **94**, 142502 (2009).
[26] Srinivasa Rao Singamaneni, Wu Fan, J. T. Prater, and J. Narayan, "Magnetic properties of BaTiO3/La0.7Sr0.3MnO3 thin films integrated on Si(100)," J. Appl. Phys. **116**, 224104 (2014).
[27] S Ramakanth and K C James Raju, "Charge transfer induced magnetism in nano crystalline BaTiO3," Solid State Commun. **187**, 59 (2014).
[28] E Orhan, J A Varela, A Zenatti, M F C Gurgel, F M Pontes, E R Leite, E Longo, P S Pizani, A Beltràn, and J Andrès, "Room-temperature photoluminescence of BaTiO3: Joint experimental and theoretical study," Phys. Rev. B **71**, 085113 (2005).
[29] Shirou Otsuki, Keishi Nishio, Tohru Kineri, Yuiichi Watanabe, and Toshio Tsuchiya, "Optical Properties of Gold-Dispersed Barium Titanate Thin Films Prepared by Sol-Gel Processing," J. Am. Ceram. Soc. **82**(7), 1676-1680 (1999).
[30] Xiaoquan Zhang, Xiaohui Wang, Zhibin Tian, Tieyu Sun, and Longtu Li, "Synthesis of Monodispersed Barium Titanate Nanoparticles with Narrow Size Distribution by a Modified Alkoxide-Hydroxide Sol-Precipitation Method," J. Am. Ceram. Soc. **93**(11), 3591-3594 (2010).
[31] Z G Hu, G S Wang, Z M Huang, and J H Chu, "Structure-related infrared optical properties of BaTiO3 thin films grown on Pt/Ti/SiO2/Si substrate," J. Phys. Chem. Solids **64**(12), 2445-2450 (2003).
[32] M. Sheik-Bahae, A. A. Said, and E. W. Vanstryland, "High-sensitivity, single-beam n2 measurements," Opt. Lett. **14**(17), 955-957 (1989).
[33] S Venugopal Rao, T Shuvan Prashant, T Sarma, K P Pradeepta, D Swain, and S P Tewari, "Two-photon and three-photon absorption in dinaphthoporphycenes," Chem. Phys. Lett. **514**, 98-103 (2011).
[34] Syed Hamad, G Krishna Podagatlapalli, Surya P Tewari, and S Venugopal Rao, "Influence of picosecond multiple/single line ablation on copper nanoparticles fabricated for surface enhanced Raman spectroscopy and photonics applications," J. Phys. D: Appl. Phys. **46**, 485501 (2013).
[35] M Yin, H P Li, S H Tang, and W Ji, "Determination of nonlinear absorption and refraction by single Z-scan method," Appl. Phys. B. **70**(4), 587-591 (2000).
[36] K Venkata Saravanan, K C James Raju, M Ghanashyam Krishna, S P Tewari, and S Venugopal Rao, "Large three-photon absorption in Ba0.5Sr0.5TiO3 films studied using Z-scan technique," Appl. Phys. Lett. **96**, 232905 (2010).
[37] Ming-Sheng Zhang, Jian Yu, Junhao Chu, Qiang Chen, and Wanchun Chen, "Microstructures and photoluminescence of barium titanate nanocrystals synthesized by the hydrothermal process'," J. Mater. Proces. Tech. **137**, 78-81 (2003).
[38] M. F. C. Gurgel, J. W. M. Espinosa, A. B. Campos, I. L. V. Rosa, M. R. Joya, A. G. Souza, M. A. Zaghete, P. S. Pizani, E. R. Leite, J. A. Varela, and E. Longo, "Photoluminescence of crystalline and disordered BTO:Mn powder: Experimental and theoretical modelling," Journal of Luminescence **126**, 771–778 (2007).
[39] Kui Woong Lee, Koppala Siva Kumar, Gaeun Heo, Maeng-Je Seong, and Jong-Won Yoon, "Characterization of hollow BaTiO3 nanofibers and intense visible Photoluminescence'," J. Appl. Phys. **114**, 134303 (2013).

[40] Natheer B. Mahmood and Emad K. Al-Shakarchi, "Three Techniques Used to Produce BaTiO3 Fine Powder'," J. Mod. Phys. **2**, 1420-1428 (2011).
[41] S. Venugopal Rao, "Picosecond nonlinear optical studies of gold nanoparticles synthesised using coriander leaves (Coriandrum sativum)," J. Mod. Opt. **58**, 1024 (2011).
[42] S. Hamad, S. P. Tewari, L. Giribabu, and S. Venugopal Rao, "Picosecond and Femtosecond Optical Nonlinearities of Novel Corroles," J. Porphy. Phth. **16**, 140 (2012).
[43] G. Krishna Podagatlapalli, Syed Hamad, Surya P. Tewari, S. Sreedhar, Muvva D. Prasad, and S. Venugopal Rao, "Silver nano-entities through ultrafast double ablation in aqueous media for surface enhanced Raman scattering and photonics applications," J. Appl. Phys. **113**, 073106 (2013).
[44] R Le Harzic, D Dörr, D Sauer, F Stracke, and H Zimmermann, "Generation of high spatial frequency ripples on silicon under ultrashort laser pulses irradiation," Appl. Phys. Lett. **98**, 211905 (2011).
[45] K Sokolowski-Tinten and D Von der Linde, "Generation of dense electron-hole plasmas in silicon," Phys. Rev. B **61**, 2643 (2000).
[46] T Kolodiazhnyi, "Insulator-metal transition and anomalous sign reversal of the dominant charge carriers in perovskite BaTiO3–δ," Phy. Rev. B **78**, 045107 (2008).
[47] Soonil Lee, Gaiying Yang, Rudeger H. T. Wilke, Susan Trolier-McKinstry, and Clive A. Randall, "Thermopower in highly reduced n-type ferroelectric and related perovskite oxides and the role of heterogeneous nonstoichiometry," Phys. Rev. B **79**, 134110 (2009).
[48] Soonil Lee, Jonathan A. Bock, Susan Trolier-McKinstry, and Clive A. Randall, "Ferroelectric-thermoelectricity and Mott transition of ferroelectric oxides with high electronic conductivity," J. Eur. Ceram. Soc. **32**(16), 3971-3988 (2012).
[49] S Ramakanth and K C James Raju, "Band gap narrowing in BaTiO3 nanoparticles facilitated by multiple mechanisms," J. Appl. Phys. **115**, 173507 (2014).
[50] B R Bennett, R A Soref, and J A D Alamo, "Carrier-induced change in refractive index of InP, GaAs and InGaAsP," IEEE J. Quantum. Elect. **26**, 113 (1990).
[51] J G M Alvarez, F D Nunes, and N B Patel, "Refractive index dependence on free carriers for GaAs," J. Appl. Phys. **51**, 4365 (1980).
[52] Weitian Wang, Liangsheng Qu, Guang Yang, and Zhenghao Chen, "Large third-order optical nonlinearity in BaTiO3 matrix-embedded metal nanoparticles," Appl. Surf. Sci. **218**, 24-28 (2003).
[53] Litty Irimpan, A. Deepthy, Bindu Krishnan, L. M. Kukreja, V. P. N. Nampoori, and P. Radhakrishnan, "Effect of self assembly on the nonlinear optical characteristics of ZnO thin films," Opt. Commun. **281**(10), 2938-2943 (2008).
[54] Chinmay Phadnis, Darshana Y. Inamdar, Igor Dubenko, Arjun Pathak, Naushad Ali, and Shailaja Mahamuni, "Ferromagnetic ZnO nanocrystals and Al-induced defects," J. Appl. Phys. **110**, 114316 (2011).
[55] Tandra Ghoshal, Tuhin Maity, Ramsankar Senthamaraikannan, Matthew T. Shaw, Patrick Carolan, Justin D. Holmes, Saibal Roy, and Michael A. Morris, "Size and space controlled hexagonal arrays of superparamagnetic iron oxide nanodots: magnetic studies and application," Sci. Reports **3**, 2772 (2013).
[56] Ying Zhang and S. Das Sarma, "Temperature and magnetization-dependent band-gap renormalization and optical many-body effects in diluted magnetic semiconductors," Phys. Rev. B **72**, 125303 (2005).
[57] Wei Qin, Xiaoguang Li, Yi Xie, and Zhenyu Zhang, "Reentrant paramagnetism induced by drastic reduction of magnetic couplings at surfaces of superparamagnetic nanoparticles," Phys. Rev. B **90**, 224416 (2014).
[58] Y. H. Matsuda, T. Ikaida, N. Miura, S. Kuroda, F. Takano, and K. Takita, "Effective mass of conduction electrons in Cd1–xMnxTe," Phys. Rev. B **65**, 115202 (2002).
[59] P M Hui, H Ehrenreich, and K C Hass, "Effects of d bands on semiconductor sp Hamiltonians," Phys. Rev. B **40**, 12346 (1989).